PERGAMON

International Journal of Solids and Structures 37 (2000) 3079–3100

INTERNATIONAL JOURNAL OF SOLIDS and STRUCTURES

www.elsevier.com/locate/ijsolstr

A finite element analysis of stationary crack tip fields in a pressure sensitive constrained ductile layer

S. Roy Chowdhury, R. Narasimhan*

Department of Mechanical Engineering, Indian Institute of Science, Bangalore, 560 012, India

Received 28 July 1998; in revised form 2 February 1999

Abstract

Polymeric ductile adhesive layers joining two elastic adherends is a common feature in various technological applications. Such joints can fail by ductile rupture involving interface debonding and void formation. It has been observed that, unlike in metals, the yield behaviour of polymers is affected by the state of hydrostatic stress. In the present study, the effect of pressure sensitivity of yielding on the stress and deformation fields near a stationary crack tip in a constrained adhesive layer is examined. To this end, finite deformation, finite element analyses of a cracked, sandwiched adhesive layer are carried out under plane strain, small-scale yielding conditions for a wide range of mode mixities. The Drucker–Prager constitutive equations are employed to represent the behaviour of the layer. Both dilational and non-dilational plastic flow are considered. It is found that the stress levels in the layer decrease with increasing pressure sensitivity irrespective of mode mixity. The effect of pressure sensitivity on the notch tip deformation, and near tip plastic mode mixity, is also investigated. Finally, theoretical predictions are made about the variation of fracture toughness with mode mixity due to interface debonding.

Keywords: Constrained ductile layer; Stationary crack tip fields; Mixed mode; Pressure sensitive yielding; Finite elements

1. Introduction

A thin ductile layer joining two elastically deforming adherends is a common architecture in various engineering applications. Some examples are laminates with alternate ceramic and metal sheets, and ceramic components which are diffusion or liquid state bonded with metal foils. Similarly, polymeric adhesive layers are employed for bonding two distinct material phases in applications such as space technology, microelectronic packaging, aerospace and automobile industry. In recent years, considerable

* Corresponding author. Tel.: +91-80-309-2589; fax: +91-80-334-1683.
E-mail address: narasi@mecheng.iisc.ernet.in (R. Narasimhan).

0020-7683/00/$ - see front matter
PII: S0020-7683(99)00046-3

attention has been focused on the fracture behaviour of such layered systems using both experimental and analytical techniques. Riemanis et al. (1991) conducted fracture experiments with gold layers sandwiched between two sapphire plates. They observed that interfacial cavities develop at distances of several times the layer thickness ahead of the crack tip with an intact ductile ligament bridging the main crack to these cavities. Varias et al. (1991, 1992) analysed a metal layer containing a midplane notch and constrained between two stiff ceramic blocks under plane strain, small-scale yielding conditions. They found that high triaxial stresses develop at locations far away from the notch tip, which leads to the cavitation observed by Riemanis et al. (1991). Roy Chowdhury and Narasimhan (1995, 1998) analysed a similar problem by employing the Gurson constitutive model (Gurson, 1977) which accounts for the ductile fracture processes of microvoid nucleation, growth and coalescence. They studied the competition between two mechanisms, namely, near-tip void coalescence and far-field triaxiality-induced cavitation, that are operative during the ductule rupture of the metal layer, for different mode mixities associated with the remote loading.

Akisanya and Fleck (1992) focused attention on polymeric adhesive systems and conducted experiments with a brittle epoxy adhesive layer sandwiched between aluminium blocks. They investigated the effect of mode mixity on the crack path and the interfacial fracture toughness. Chai (1986) studied the effect of bond thickness on the fracture energy from tests performed using brittle and ductile adhesive systems under Mode I loading. He found a complete correlation in the fracture behaviour of laminated composites and thin-bond joints and, thus, established the latter as a viable alternative to composite fracture testing and analysis. Chai (1992, 1993) conducted experiments to investigate the micromechanics of deformation and damage at the crack tip in adhesive bonds under shear loading (Mode II). He found that the plastic deformation zone in the layer extends to distances which are several orders of magnitude greater than the bond thickness. Chiang and Chai (1994, 1998) analysed the fracture specimens employed in the earlier experiments of Chai (1992, 1993) using the finite element method. Thus, they considered only shear (Mode II) loading in their analyses.

A systematic investigation of stationary crack tip fields in a polymeric adhesive layer which exhibits pressure sensitive yielding has not been reported in the literature. The studies by Varias et al. (1991, 1992) pertain to constrained metal layers obeying the J_2 flow theory of plasticity in which hydrostatic stress does not affect yielding. On the other hand, it is well known that yield behaviour in polymers depends on the level of the hydrostatic stress (see, for example, Bowden and Jukes, 1972). Li and Pan (1990a, b) investigated the crack tip fields for a pressure sensitive, homogeneous (unconstrained), ductile material under Mode I, plane-strain and plane-stress conditions. They obtained HRR type solutions (Hutchinson, 1968; Rice and Rosengren, 1968) and observed that the magnitude of the hydrostatic stress ahead of the crack tip decreases with increasing pressure sensitivity of the material. Further, Dong and Pan (1991) showed from a finite element analysis that both the size and shape of the plastic zone in a homogeneous material are strongly influenced by the level of pressure sensitivity under Mode I loading. In view of these observations, it becomes necessary to study the effects of pressure dependence of yield on the crack tip fields in a constrained adhesive layer. In particular, the hydrostatic stress levels observed by Varias et al. (1991, 1992) may be diminished by the pressure sensitivity of the layer. This will also reflect in the theoretical predictions of fracture toughness made in the above studies. It must be mentioned that Chiang and Chai (1994) in their finite element analyses of adhesively bonded fracture specimens observed that the plastic zone length and shear strain in the layer are little affected by the pressure sensitivity. However, their analysis was limited to (remotely applied) pure Mode II loading conditions and other levels of mode mixity have not been considered.

Thus, the main objective of the present work is to investigate the effect of pressure sensitive yielding on the stress and deformation fields in a ductile polymeric layer bonding two elastic adherends. To this end, finite deformation, finite element analyses of a cracked sandwiched layer are carried out under plane strain, small-scale yielding conditions for the full range of mode mixities from (remote) Mode I to

II. Pressure dependence is accounted for by the Drucker–Prager yield criterion (see Section 2.1). Analyses are carried out for both dilational and non-dilational flow rule. The effect of pressure sensitivity on the plastic zone size, stresses ahead of the tip, notch tip deformation and near-tip plastic mode mixity is examined. Finally, following Varias et al. (1992), initiation of debonding along the interface is considered based on a critical effective stress criterion. Theoretical predictions are made on the variation of fracture toughness with mode mixity for both pressure sensitive and pressure insensitive materials.

2. Numerical analysis

2.1. Constitutive equations

Experimental evidence suggests that yield behaviour of polymeric materials is considerably different from that of metals. In particular, the yield stress under uniaxial tension for a polymer is different from that in uniaxial compression (see, for example, Bauwens, 1970; Bowden and Jukes, 1972). It has also been observed that the bands appearing during plastic deformation depart from the plane of maximum shear stress (Argon et al., 1968). Such behaviour can be explained by assuming a pressure-dependent yield criterion. Consequently, three such criteria, namely, Drucker–Prager, Mohr–Coulomb and modified Tresca (Bowden and Jukes, 1972) have been suggested to describe yielding in polymeric solids. The essential feature of these criteria is that the yield stress exhibits a linear dependence on hydrostatic stress. The appropriateness of employing one of the above yield criteria depends largely on the deformation mode exhibited by the polymer. Thus, the yield behaviour of polymers which exhibit heterogeneous deformation by shear banding during plastic deformation [such as polystyrene (PS), polyethylene terephthalate (PET)] is closely approximated by Mohr–Coulomb or modified Tresca criterion. On the other hand, the Drucker–Prager yield criterion is suitable for polymers which undergo a more homogeneous plastic deformation such as polymethyl methacrylate (PMMA), polyvinyl chloride (PVC), epoxy resins, etc. (Bauwens, 1970; Bowden and Jukes, 1972; Quinson et al., 1997).

From the standpoint of a numerical formulation, it is easier to implement the Drucker–Prager yield criterion, since it has a continuously varying normal. Moreover, it can be extended in such a way that with proper selection of different parameters it closely approximates the Mohr–Coulomb yield criterion (Abaqus, 1996). Hence, in this work, an extended Drucker–Prager (EDP) model is employed to describe the constitutive response of the polymeric adhesive layer. The EDP yield function is given as (see Abaqus, 1996):

$$\Phi(\sigma_{ij}, \sigma^{c}) = \frac{q}{2}\left[1 + \frac{1}{C} - \left(1 - \frac{1}{C}\right)\left(\frac{r}{q}\right)^{3}\right] + \sigma_m \tan\alpha - \left(1 - \frac{1}{3}\tan\alpha\right)\sigma^{c} = 0, \tag{1}$$

where

$$\sigma_m = \tfrac{1}{3}(\sigma_1 + \sigma_2 + \sigma_3),$$

$$q = \sqrt{(3J_2)},$$

and,

$$r^3 = \tfrac{27}{2}J_3.$$

Here, (σ_1, σ_2, σ_3) are the principal values of the Cauchy stress tensor σ_{ij}, J_2 and J_3 are the second and third invariants of the deviatoric part of the Cauchy stress, and σ_m is the hydrostatic stress. Further, σ^c is the true yield stress in a uniaxial compression test and α and C are material parameters. The yield function described by Eq. (1) represents a conical surface in principal stress space with the vertex on the hydrostatic tension axis. The trace of the yield surface on the deviatoric plane is non-circular and its shape is determined by the parameter C. A circular trace is obtained for the special case of $C = 1$ which corresponds to the original Drucker–Prager model. To ensure convexity of the yield surface, C must be chosen greater than 0.778 (Abaqus, 1996). It must be noted that for the case $C = 1$ and $\alpha = 0^\circ$, Φ in Eq. (1) reduces to the Huber–von Mises yield function.

On applying the yield criterion (1) for uniaxial tension and uniaxial compression, it can be shown that

$$\tan\ \alpha = 3\left(\lambda - \frac{1}{C}\right)/(\lambda + 1), \tag{2}$$

where $\lambda = \sigma^c/\sigma^t$ is the ratio of the (true) yield stress in uniaxial compression to that in uniaxial tension. The value of λ varies in the range 1.1 to 1.2 for most polymers (Brown, 1987).

The total deformation rate D_{ij} (symmetric part of the spatial gradient of velocity) is taken to be the sum of an elastic and a plastic part, so that,

$$D_{ij} = D^e_{ij} + D^p_{ij}. \tag{3}$$

The Jaumann rate of Cauchy stress σ^*_{ij} is related to D^e_{ij} by a constant, positive definite, isotropic elasticity tensor L_{ijkl} as

$$\sigma^*_{ij} = L_{ijkl} D^e_{kl}. \tag{4}$$

The plastic volume change observed in polymers is generally less than that predicted by the associated flow rule. For example, Chiang and Chai (1994) observed, from an analysis performed on a model shear specimen, that an adhesive layer exhibits plastic volume change of over 100% for the case of associated flow with $\alpha \approx 20^\circ$. Hence, a non-associated flow rule is employed here. The plastic part of the deformation rate D^p_{ij} is directed along the normal of a flow potential G, which is given by

$$G(s_{ij}) = \frac{q}{2}\left[1 + \frac{1}{C} - \left(1 - \frac{1}{C}\right)\left(\frac{r}{q}\right)^3\right] + \sigma_m\ \tan\beta. \tag{5}$$

On comparing Eqs. (1) and (5), it can be seen that for the case $\beta = \alpha$, the normals to the yield surface and flow potential surface in stress space coincide resulting in associated plastic flow, whereas $\beta \neq \alpha$ leads to non-associated flow. In particular, $\beta = 0^\circ$ results in non-associated and non-dilational plastic flow. In order to describe the strain hardening behaviour, an effective plastic strain increment is first defined as

$$\mathrm{d}\bar{\epsilon}^p = \frac{(1 - \frac{1}{3}\ \tan\ \beta)}{\sqrt{\frac{3}{2} + \frac{1}{3}\ \tan^2\beta}}\sqrt{D^p_{ij} D^p_{ij}}, \tag{6}$$

so that it reduces to the axial plastic strain increment under uniaxial compression. The slope of the true stress vs true plastic strain curve under uniaxial compression, $\mathrm{d}\sigma^c/\mathrm{d}\bar{\epsilon}^p$, is denoted by H_m. On employing Eq. (4) along with the flow rule and the plastic consistency condition, the rate constitutive equation can be derived as,

$$\sigma^*_{ij} = M_{ijkl} D_{kl}, \tag{7}$$

where M_{ijkl} is the elastic–plastic constitutive tensor.

The response of the polymeric material in uniaxial compression is idealized here by a piecewise power hardening law of the form:

$$\frac{\epsilon^c}{\epsilon^c_0} = \begin{cases} \sigma^c/\sigma^c_0 & \sigma^c \le \sigma^c_0 \\ (\sigma^c/\sigma^c_0)^n & \sigma^c > \sigma^c_0 \end{cases}. \tag{8}$$

Here, σ^c_0 is the initial yield stress and $\epsilon^c_0 = \sigma^c_0/E$ is the initial yield strain under uniaxial compression and n is the strain hardening exponent of the material.

2.2. Modelling aspects

In this work, a system comprising of two identical semi-circular elastic adherends, joined by a thin polymeric adhesive layer of thickness h containing a mid-plane notch, is considered. Plane strain, small-scale yielding conditions are assumed to prevail. As shown in Fig. 1(a), a circular domain with radius $R \approx 3900h$ is modelled with four-noded isoparametric quadrilateral finite elements. An overall view of the finite element discretization is shown in Fig. 1(a). An enlarged view of the region near the interface between the adhesive layer and the elastic adherends is displayed in Fig. 1(b). This is surrounded by the mesh given in Fig. 1(a). Fig. 1(c) shows the details of the highly refined mesh in the region close to the notch tip. The initial diameter of the notch, b_0, is taken as $0.02h$. The average dimension of the smallest element close to the notch in Fig. 1(c) is around $b_0/7$. A set of Cartesian axis X_1, X_2, established with origin at the centre of curvature O of the notch in the undeformed configuration, is shown in Fig. 1(c).

The displacement field corresponding to the dominant term of the mixed mode linear elastic solution,

$$\hat{\mathbf{u}} = \frac{K_I}{2\mu}\sqrt{\frac{r}{2\pi}}\hat{\mathbf{u}}^I(\theta) + \frac{K_{II}}{2\mu}\sqrt{\frac{r}{2\pi}}\hat{\mathbf{u}}^{II}(\theta) \tag{9}$$

is specified as the boundary condition on the outermost boundary S (see Fig. 1(a)). In the above equation, K_I and K_{II} are the Mode I and II elastic stress intensity factors, respectively, μ is the elastic shear modulus of the adherends, and r, θ are polar coordinates in the undeformed state with origin at O. The functions $\hat{\mathbf{u}}^I(\theta)$ and $\hat{\mathbf{u}}^{II}(\theta)$ are given by Kanninen and Popelar (1985). The simulations are carried out for different combinations of the material parameters α, β and the mode mixity parameter $\psi = \tan^{-1}(K_{II}/K_I)$. The load is applied by gradually increasing the effective stress intensity factor $|K| = \sqrt{K_I^2 + K_{II}^2}$ while maintaining a constant value of ψ. An updated Lagrangian finite element procedure (McMeeking and Rice, 1975), in which the reference configuration coincides instantaneously with the current configuration, is employed in this work. The accuracy of the computations is continuously monitored by checking the magnitude of the out-of-balance forces which signify the deviation from equilibrium.

The maximum extent of the plastic zone surrounding the notch tip in the adhesive layer is always contained within 1/20th of the radius R, so that small-scale yielding conditions are preserved. All plastic deformation in the adhesive layer is confined within the active region shown in Fig. 1(a). The constant stiffness of the elastic region surrounding the active mesh is statically condensed using a ring-by-ring static condensation method.

A mesh convergence study was undertaken to verify the accuracy of the results. To this end, some analyses were repeated with a mesh which had approximately two and half times more elements than that depicted in Fig. 1. Special attention was focused on the notch tip zone, where the elements in the refined mesh were one-fourth in size of the corresponding elements in the original mesh. The results

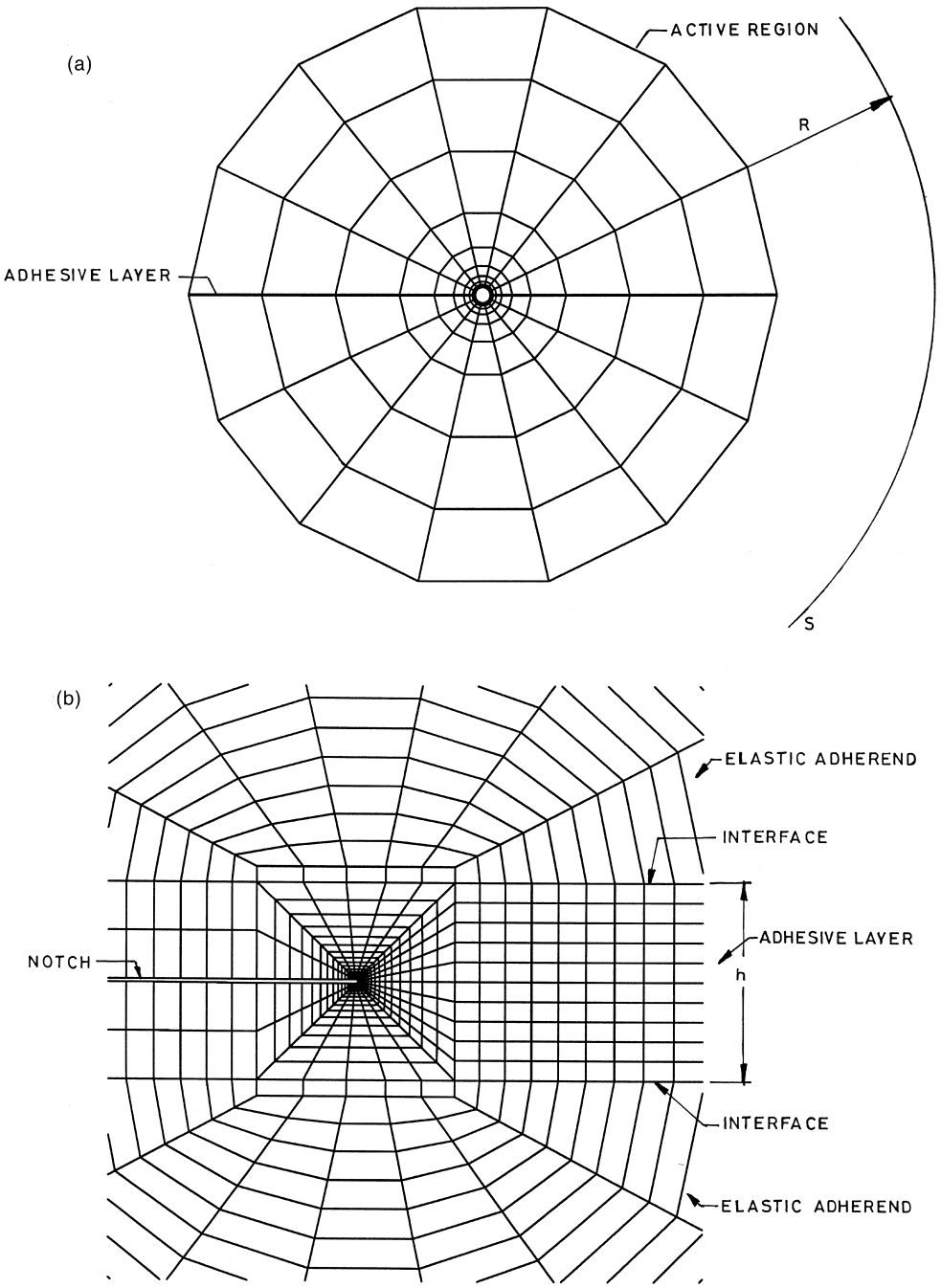

Fig. 1. (a) Overall view of the mesh used in the finite element analysis. (b) View of the mesh near the interface region between the adhesive layer and the elastic adherends. The thickness of the layer, h, is indicated in the figure. (c) Details of the mesh near the notch tip region.

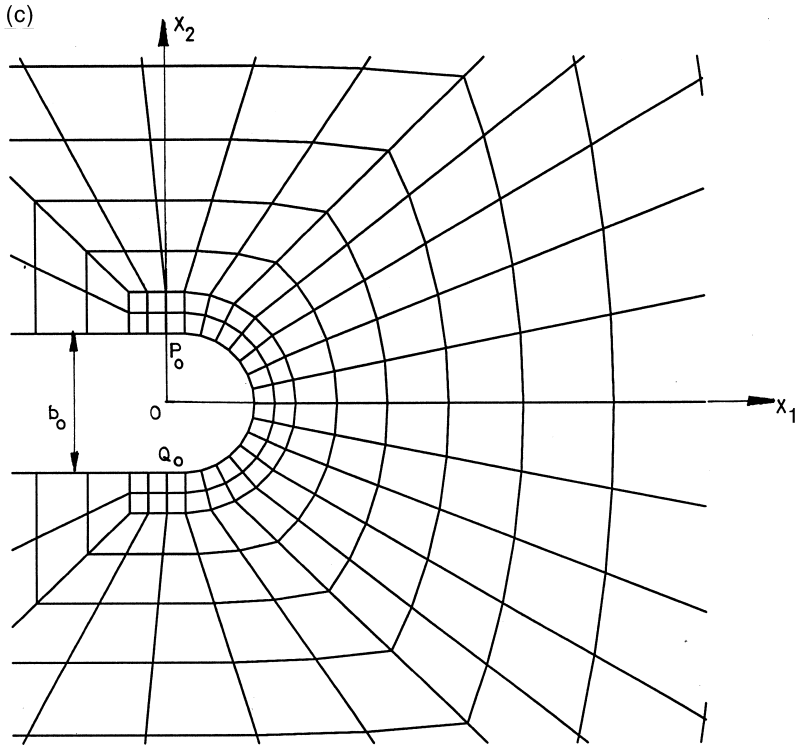

Fig. 1 (*continued*).

obtained from the two different meshes were almost the same. For example, a maximum difference of 6% was observed in the stress and strain distributions ahead of the notch tip. Thus, it can be concluded that reasonably converged results are obtained using the mesh shown in Fig. 1.

2.3. Material properties

In the present work, the uniaxial compressive behaviour of the adhesive layer is assumed to follow Eq. (8) with $n = 10$, $E/\sigma_0^c = 300$ and Poisson's ratio $\nu = 0.36$. Since the stiffness of the elastic adherends is expected to be considerably higher than the adhesive layer, their Young's modulus is assumed as $E_s = 20E$, and $\nu_s = 0.3$. It should be mentioned that the yield characteristics in polymers are affected by temperature and strain rate. To a first approximation, the yield point shows linear variation with temperature and natural logarithm of strain rate (Argon et al., 1968; Brown, 1987). However, such effects are not considered here, because the primary focus of this work is on the effect of pressure sensitive yielding on the crack tip fields in the adhesive layer. In other words, an isothermal, quasistatic loading of the layer is assumed in this work.

Experimental investigations on the effect of hydrostatic stress on yielding suggest that for polymeric materials, α is usually less than 23° (Bowden and Jukes, 1972; Quinson et al., 1997; Brown, 1987). Accordingly, in this work, most analyses are carried out for $\alpha = 0$, 10 and 20°. On the other hand, there is a general scarcity of data in literature regarding appropriate values of β for polymeric materials. However, it has been observed in experiments that polymers undergo some volume change during plastic deformation. The extent of dilatancy, though small, varies for different polymers (Pampillo and

Davis, 1971; Wang et al., 1982; Brady and Yeh, 1971). In the present computations, the flow parameter β which affects the plastic volume change is taken in the range 0° to α. It must be noted that, while the case $\beta=\alpha$ represents a dilational associated flow, no plastic volume change takes place for $\beta=0^\circ$. The value of the parameter C in Eq. (1) is taken as unity for all the analyses, since it was found from some trial computations that perturbation of C from 0.8 to 1.0 has little influence on the stresses in the adhesive layer.

It should be mentioned here that the E/σ_0^c value chosen in the present analysis is larger than that for polymers (see, for example, Brown, 1987). This is because it was observed that for a very low E/σ_0^c ratio, the deformation is highly localised near the notch tip. This high strain concentration distorts the mesh near the notch tip to a large extent and makes analysis over a reasonable load range impossible. Hence, a higher value of E/σ_0^c is selected. However, some analyses are conducted to study the effect of the above parameter on the results presented here. It is found that the general trends in the results to be discussed in Section 3 are not significantly affected by E/σ_0^c (see, in particular, Section 3.7).

3. Results and discussion

Results pertaining to the plastic zone size and the stress and deformation fields in the adhesive layer are presented below for Mode I and mixed mode loading conditions. The effect of yield and flow parameters on the above fields is investigated. Finally, the variation of the critical value of a normalised load parameter at fracture initiation due to interface debonding, with mode mixity is predicted.

The adhesive layer thickness, h, is a natural length scale in the geometry considered which pertains to a boundary layer formulation with a semi-infinite crack. Moreover, for most of the analyses reported here, the notch tip experiences predominantly tensile loading (see Section 3.4). Thus, the parameter $(|K|/\sigma_0^t)^2$ is another natural length scale associated with the yield strength of the layer and is a measure of the size of the plastic zone. Here, σ_0^t (given by σ_0^c/λ) is the yield stress under uniaxial tension. Due to these reasons, the parameter $|K|/(\sigma_0^t h^{1/2})$ seems to present itself as a natural nondimensional load parameter for the problem.

The suitability of the above parameter was separately verified by performing some elastic–plastic analyses with a finite width, adhesively bonded specimen geometry for different thicknesses. It was observed from these analyses that, provided small scale yielding conditions apply, the stress field ahead of the notch tip at the same $|K|/(\sigma_0^t h^{1/2})$ is invariant with respect to the thickness h of the layer. This confirms that $|K|/(\sigma_0^t h^{1/2})$ is indeed a valid load parameter for the present problem.

3.1. Contours of effective plastic strain

Figs. 2(a) and (b) show the contours of effective plastic strain [see definition given in Eq. (6)] for $\alpha=\beta=20^\circ$ corresponding to $\psi=0$ and 60°, respectively. Both these figures pertain to $|K|/(\sigma_0^t h^{1/2})=13.9$. It can be observed from these figures that the plastic strain ahead of the notch tip is much lower for $\psi=0^\circ$ as compared to that for $\psi=60^\circ$. Moreover, for Mode I loading, the plastic strain contours spread towards the interfaces, whereas for predominantly Mode II loading they progress more in front of the notch tip and are confined to the mid-plane of the layer. Thus, the plastic zone is expected to grow more rapidly for mixed-mode loading. This phenomenon and its consequences will be discussed in more detail in the following sections.

3.2. Variation of plastic zone with load

Following Varias et al. (1992), the plastic zone size r_p in the layer is defined here as the maximum

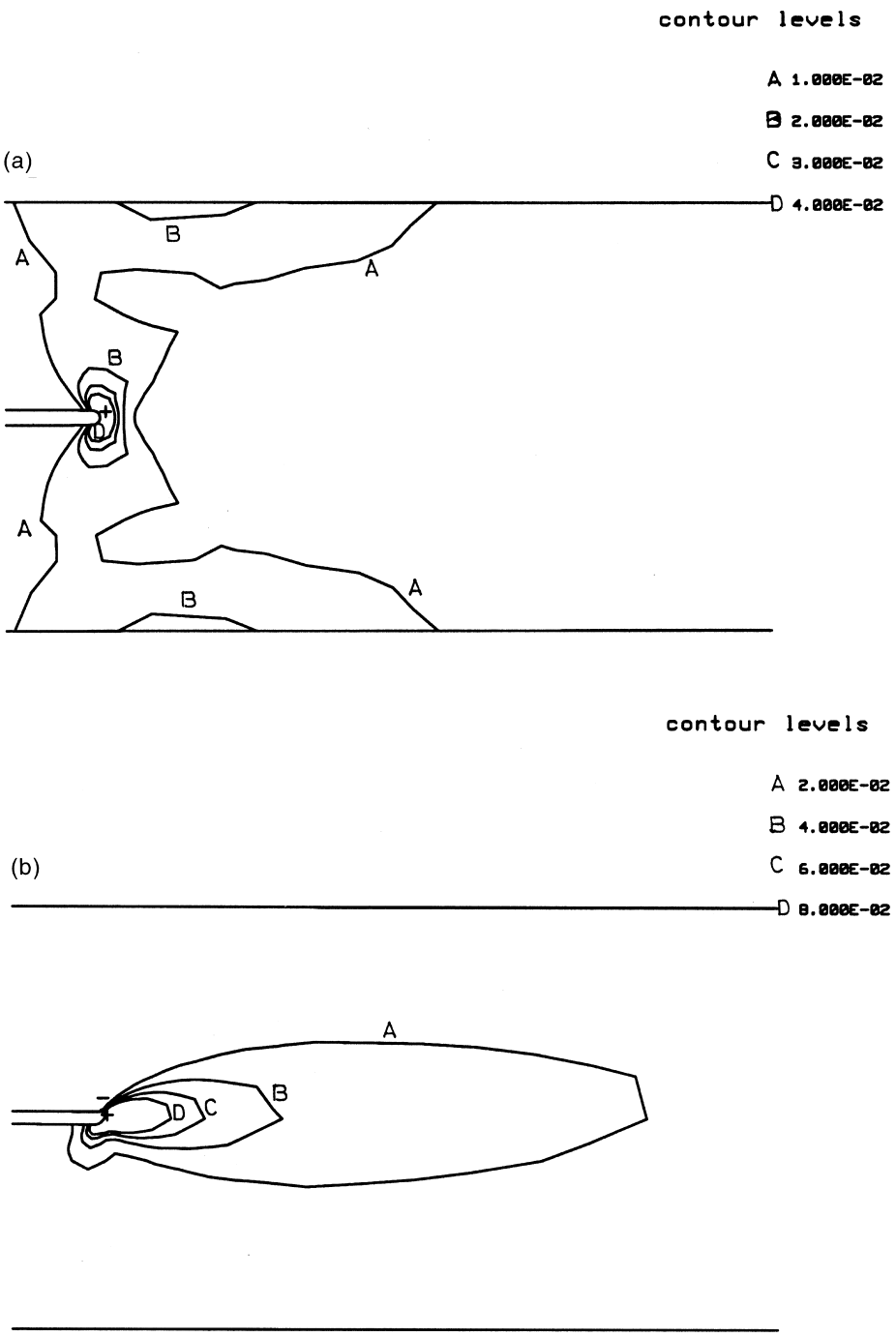

Fig. 2. Contours of effective plastic strain at $|K|/(\sigma_0^t h^{1/2}) = 13.9$ corresponding to $\alpha = \beta = 20^\circ$ for (a) $\psi = 0^\circ$ and (b) $\psi = 60^\circ$.

distance of the effective plastic strain contour $\bar{\epsilon}^{p} = 0.001$ from the notch tip. In Figs. 3(a) and (b) the variation of r_p/h with applied load $|K|/(\sigma_0^t h^{1/2})$ is shown for $\psi = 0$ and 60° for different values of α. These figures pertain to associated plastic flow (i.e., $\alpha = \beta$) of the layer. It can be observed from Fig. 3(a) that for the Mode I case, the plastic zone grows faster with respect to load when α increases from 0° (i.e., when the material behaviour of the layer deviates further from the Von Mises type yield condition). A similar observation was made by Dong and Pan (1991) for a pressure sensitive (unconstrained) homogeneous elastic–plastic solid. In fact, Fig. 3(a) shows that the difference in r_p/h between the case $\alpha = 0^\circ$ and $\alpha > 0^\circ$ becomes quite large at higher loads. For example, it can be observed from this figure that corresponding to $\psi = 0^\circ$, the difference in r_p between $\alpha = 20$ and 0° is about $3.3h$ at $|K|/(\sigma_0^t h^{1/2}) = 10$, whereas, it increases to around $7h$ at $|K|/(\sigma_0^t h^{1/2}) = 14$. On the other hand, Fig. 3(b) shows that for $\psi = 60^\circ$ there is very little effect of α on the variation of r_p/h with respect to $|K|/(\sigma_0^t h^{1/2})$. This trend is in

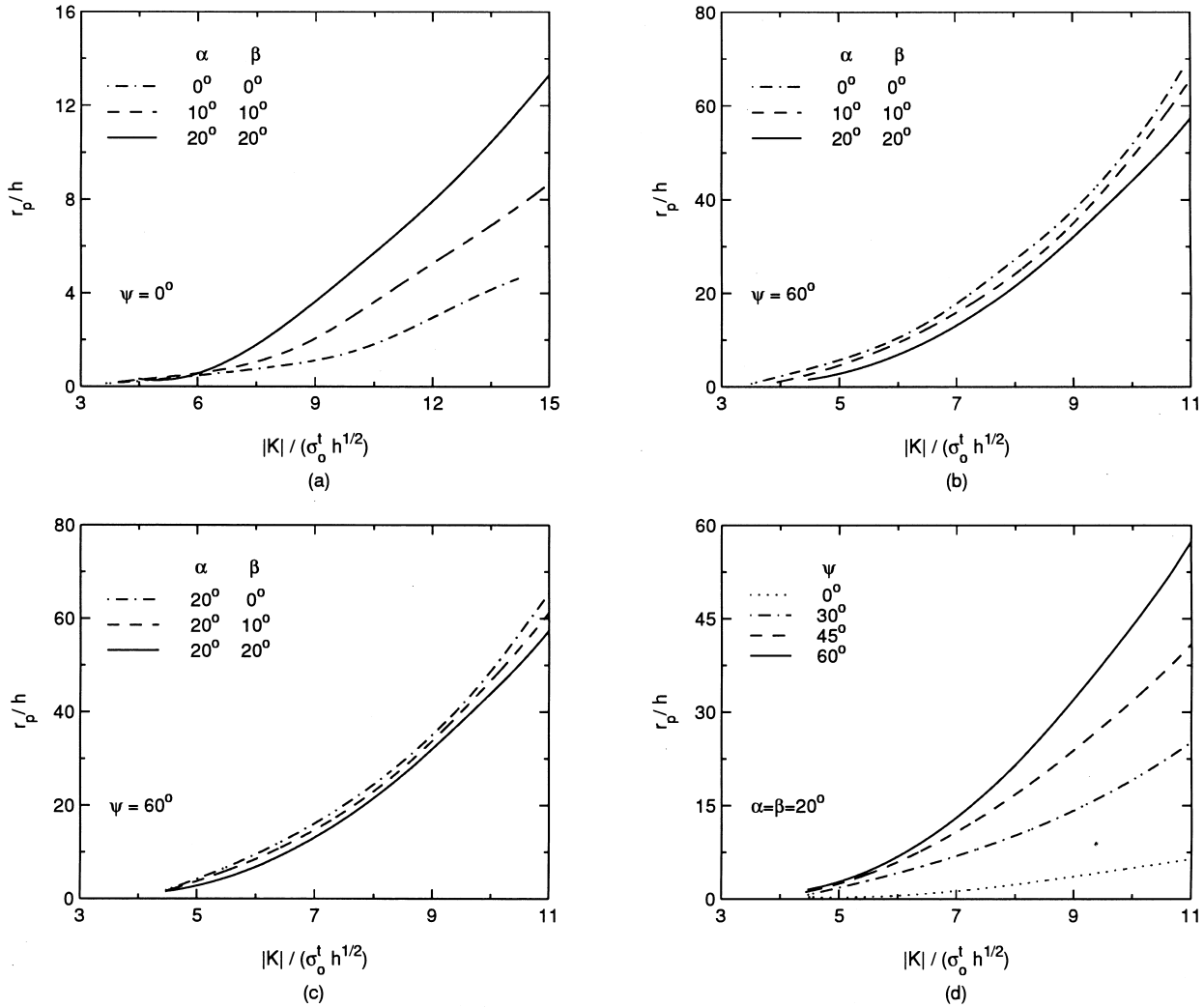

Fig. 3. Variations of normalised plastic zone size r_p/h with normalised applied load $|K|/(\sigma_0^t h^{1/2})$ for different levels of α and β corresponding to (a) $\psi = 0^\circ$ and (b, c) $\psi = 60^\circ$. (d) Effect of mode mixity parameter ψ on the plastic zone size for the case $\alpha = \beta = 20^\circ$.

agreement with Chiang and Chai (1994) who observed that the plastic zone size is not much affected by the parameter α under pure Mode II loading.

In order to examine the effect of non-associated plastic flow (i.e., $\alpha \neq \beta$) on the growth of the plastic zone in the adhesive layer, the variations of r_p/h with $|K|/(\sigma_0^t h^{1/2})$ are presented corresponding to several values of β but with a fixed $\alpha = 20^\circ$ in Fig. 3(c). This figure pertains to the mode mixity parameter $\psi = 60^\circ$. It must be recalled that for $\beta = 0^\circ$, the plastic flow is non-dilational, whereas for $\beta > 0^\circ$ it is dilational. It can be seen from Fig. 3(c) that change in β has little effect on the growth of the plastic zone with respect to $|K|/(\sigma_0^t h^{1/2})$. Finally, the influence of mode mixity parameter ψ on the variation of r_p/h with $|K|/(\sigma_0^t h^{1/2})$ is shown in Fig. 3(d) corresponding to a pressure sensitive adhesive layer with $\alpha = \beta = 20^\circ$. It can be observed that at a fixed $|K|/(\sigma_0^t h^{1/2})$, the plastic zone size is lowest for Mode I and increases strongly with increase in Mode II component (i.e., with increase in ψ), which is akin to a pressure insensitive layer (Varias et al., 1992).

It should be noted here that although the size of the plastic zone, r_p, is quite large compared to the thickness of the adhesive layer, h, yielding is confined to within 1/20th of the radius, R, of the outer boundary S (see Fig. 1(a)). Thus small scale yielding conditions are preserved throughout the analysis.

3.3. Stress fields

The normalized opening stress, σ_{22}/σ_0^t, along the midplane of the layer, is plotted as a function of normalised distance from the notch tip in the undeformed configuration, X_1/h, for the Mode I case in Figs. 4(a)–(d). Figs. 4(a)–(c) pertain to associated flow with various levels of α, whereas Fig. 4(d) pertains to a case of non-associated flow with $\alpha = 20^\circ$, $\beta = 0^\circ$. Results are presented corresponding to identical load levels $|K|/(\sigma_0^t h^{1/2})$ in these figures to facilitate easy comparison. It can be seen from Fig. 4(a), which corresponds to $\alpha = \beta = 0^\circ$, that two peaks develop in the distribution of the opening stress ahead of the notch. The first peak is very close to the tip, attains a value around 3.5 and is relatively unaffected by the level of the applied load. On the other hand, both the magnitude and the location of the second peak are strongly affected by the load level. As discussed by Varias et al. (1992) and Roy Chowdhury and Narasimhan (1998), the second peak can considerably influence the failure process in the layer.

On comparing Fig. 4(a) with Fig. 4(b) and (c), it can be observed that with increasing degree of pressure sensitivity (i.e., larger α), the normal stress level in the adhesive layer decreases. In particular, the magnitude of the second peak in the variation of σ_{22}/σ_0^t with X_1/h reduces as α increases. Moreover, the second peak occurs at a location further ahead of the notch tip and becomes less sharp with increase in α. These effects can be more clearly perceived as α increases from 10 to 20° (see Fig. 4(b) and (c)). On comparing Fig. 4(c) and (d) (which pertain to the same α), it can be observed that for the Mode I case the flow parameter β has very little influence on the stress distribution ahead of the notch tip.

The variation of hydrostatic stress σ_m (normalised by σ_0^t) with X_1/h along the midplane of the adhesive layer under Mode I loading ($\psi = 0^\circ$), corresponding to different values α for the case of associated plastic flow, is shown in Fig. 5. This figure pertains to a normalised load level of $|K|/(\sigma_0^t h^{1/2}) = 18.0$. Fig. 5 shows that, as in the case of the normal stress, the peak hydrostatic stress also decreases as α increases from 0 to 20° and its location shifts further away from the notch. Again, this effect is more pronounced as α increases from 10 to 20°. Since for most adhesives α varies from 9 to 23° (Bowden and Jukes, 1972; Quinson et al., 1997), the above trends imply that for a fracture mechanism (like interface debonding) which is strongly influenced by stress levels, the fracture toughness of the system would exhibit marked dependence on the pressure sensitive nature of the adhesive layer (see Section 3.6).

It was found that under mixed mode loading, the stress levels at the lower interface are always higher than that at the upper interface. In fact, for a remote loading very close to Mode II, a state of

hydrostatic compression prevails at the upper interface region. Hence, the distribution of σ_{22}/σ_0^t and σ_m/σ_0^t with X_1/h along the lower interface ($X_2=-h/2$) for the mixed mode case $\psi=60^\circ$ are shown in Fig. 6(a) and (b), respectively, at a normalised load level of $|K|/(\sigma_0^t h^{1/2})=13.9$. Results are presented for different values of α for the case of associated plastic flow ($\alpha=\beta$). On comparing Figs. 4 and 5 with Fig. 6(a) and (b), it can be observed that the stress levels are much lower for $\psi=60^\circ$. Further, unlike $\psi=0^\circ$, the stresses decrease monotonically after the first peak, which occurs at distances very close to the notch tip. However, similar to $\psi=0^\circ$, the stress levels reduce as α is changed from 0 to 20° under mixed mode loading (see Fig. 6(a) and (b)). But, unlike the Mode I case, it was found that under mixed mode loading, decrease in the flow parameter β elevates the normal stress in the layer.

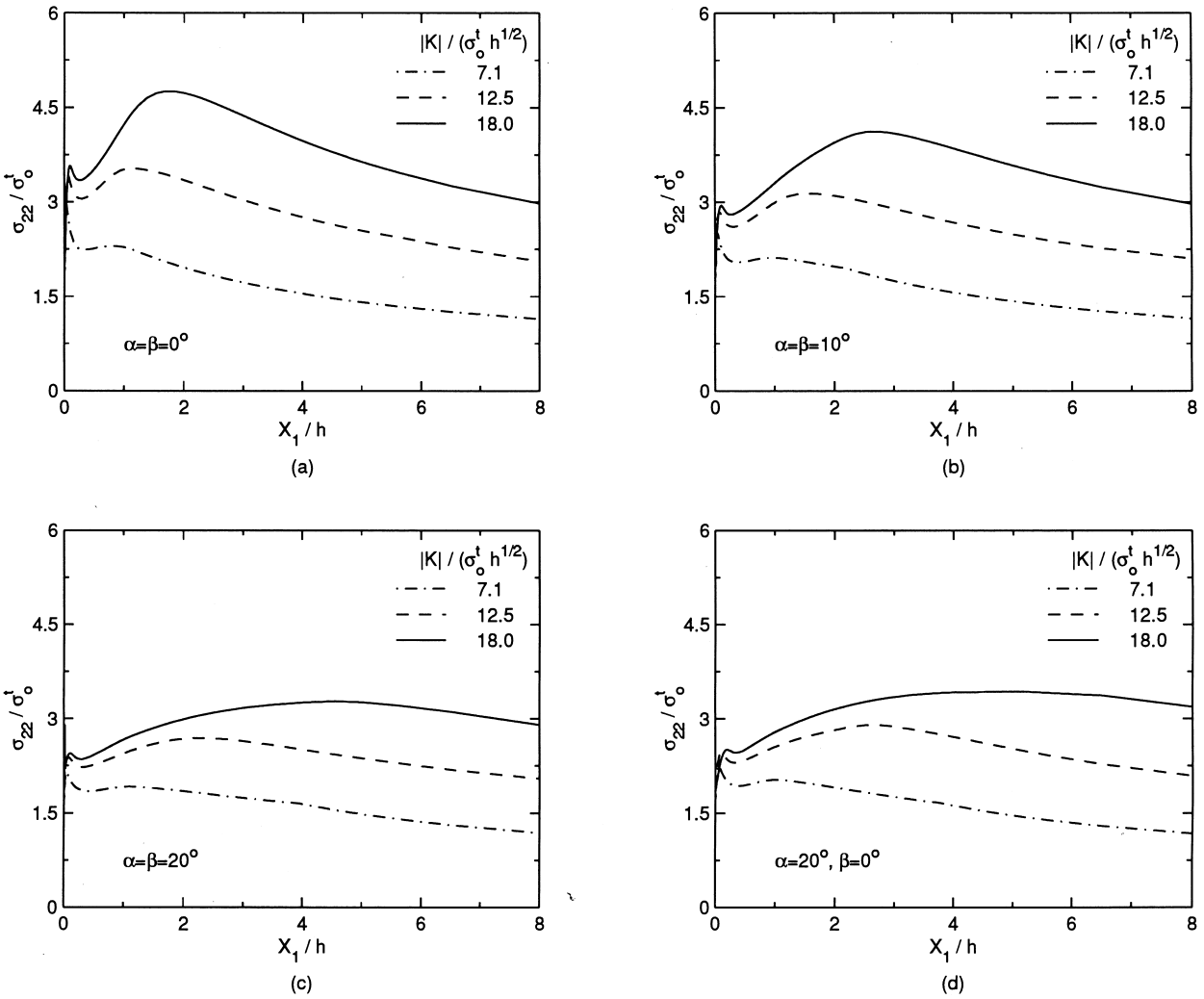

Fig. 4. Variations of normalised stress σ_{22}/σ_0^t with normalised distance in the undeformed configuration, X_1/h, along the mid-plane of the adhesive layer at different load levels for $\psi=0^\circ$ corresponding to (a) $\alpha=\beta=0^\circ$, (b) $\alpha=\beta=10^\circ$, (c) $\alpha=\beta=20^\circ$ and (d) $\alpha=20^\circ$, $\beta=0^\circ$.

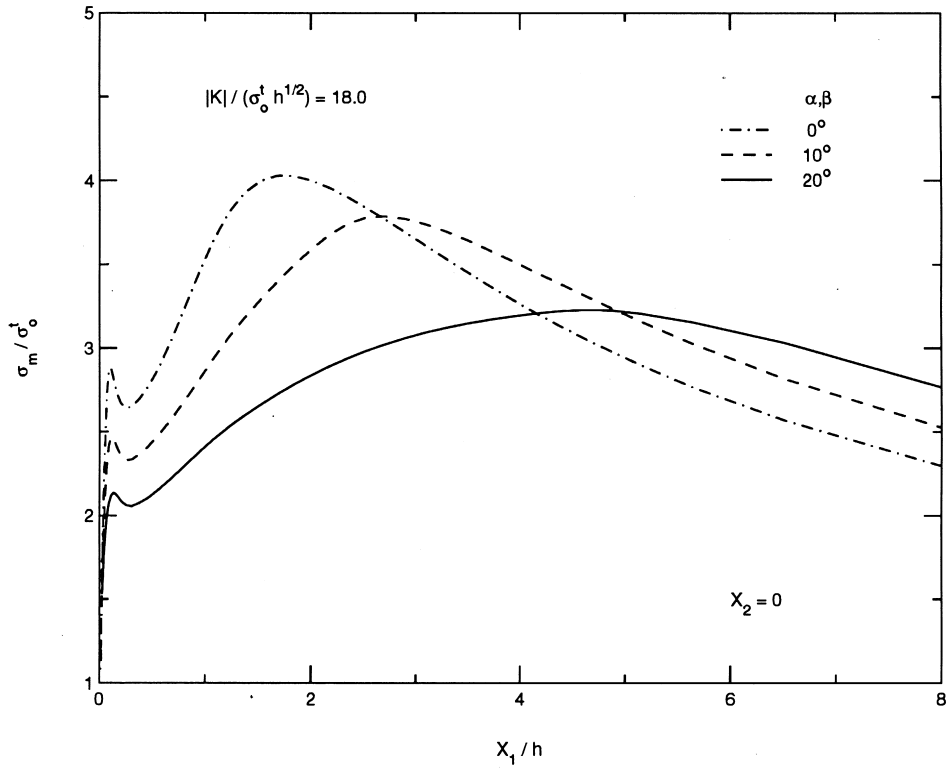

Fig. 5. Variation of normalised hydrostatic stress σ_m/σ_0^t with normalised distance in the undeformed configuration, X_1/h, along the mid-plane of the adhesive layer for $\psi = 0^\circ$ corresponding to different levels of α, β at a fixed load.

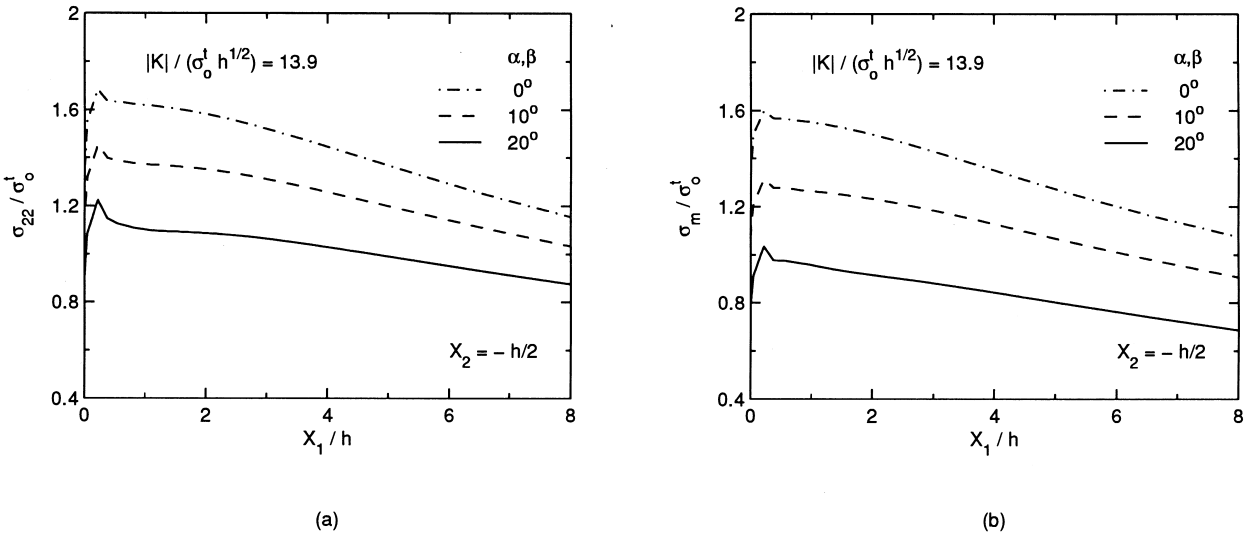

Fig. 6. Variations of normalised stresses with normalised distance along the lower interface for $\psi = 60^\circ$, (a) σ_{22}/σ_0^t vs X_1/h (b) σ_m/σ_0^t vs X_1/h.

3.4. Near-tip plastic mode mixity

It is quite well known that plasticity causes the mode mixity near the notch tip to be different from that associated with the far-field loading. Shih (1974) demonstrated that the asymptotic fields under mixed mode loading in a homogeneous elastic–plastic solid are scaled by the J integral and parameterized by the plastic mode mixity (see definition below) prevailing near the crack tip. He also obtained the relationship between the near-tip plastic mixity and the remote elastic mixity (denoted here as ψ) for a homogeneous material obeying the J_2 flow theory of plasticity under small-scale yielding conditions. In the following, the above relationship is investigated in some detail for pressure insensitive and pressure sensitive adhesive layers.

To this end, a mode mixity parameter ψ_p is defined as

$$\psi_p = \tan^{-1}(\sigma_{12}/\sigma_{22})\,|_{X_2=0}\,. \tag{10}$$

Thus, $\psi_p = 0$ and 90° correspond to Mode I and II conditions, respectively. The variation of ψ_p (in degrees) with normalised distance X_1/h ahead of the notch tip, at different load levels, is shown in a semilog plot in Fig. 7(a). A logarithmic axis is used for the abscissa in order to accommodate length scales that differ by over three orders of magnitude. This figure corresponds to a pressure insensitive layer ($\alpha = \beta = 0^\circ$) and a remote elastic mode mixity of $\psi = 60^\circ$. It can be seen from this figure that for all cases, $\psi_p \to \psi$ at larger distances from the notch tip, which is an essential condition for small scale yielding. As the notch tip is approached from the outer boundary, ψ_p decreases from the remote elastic mixity ψ, but attains an almost constant limit in the range $X_1 \leq 3h$. This asymptotic limit is denoted here by ψ_p^a. It can be noticed from Fig. 7(a) that ψ_p^a is a function of the applied load level. The above observations are common to all combinations of remote mixity and material parameters.

The variation of ψ_p^a with the normalised load parameter $|K|/(\sigma_0^t h^{1/2})$ for different remote elastic mode mixities ψ is plotted in Fig. 7(b) and (c) for a pressure insensitive ($\alpha = \beta = 0^\circ$), and a pressure sensitive ($\alpha = \beta = 20^\circ$) adhesive layer, respectively. The near-tip plastic mixities in an unconstrained, pressure insensitive, homogeneous solid (with $n = 10$) corresponding to remote elastic mixities of $\psi = 0$, 30, 65, 75 and 90° are 0, 18, 45, 65 and 90°, respectively (Shih, 1974). It can be observed from Fig. 7(b), that for a pressure insensitive constrained layer, ψ_p^a differs from that in a homogeneous material except for $\psi = 0$ and 90°. In most cases, for the same remote mixity ψ, the stress state near the notch tip is closer to Mode I conditions for a constrained layer compared to a homogeneous material. Further ψ_p^a decreases with increasing load, and thus tends even closer to Mode I. The above result is attributed to higher normal (and triaxial) stress in the layer due to constrained plastic flow.

On comparing Fig. 7(b) and (c), it can be observed that ψ_p^a for a pressure sensitive layer is somewhat different from that for the pressure insensitive case. For a remote mixity of $\psi = 30^\circ$, the mixity near the tip for $\alpha = \beta = 20^\circ$ is less than that for $\alpha = \beta = 0^\circ$ at similar loads. For $\psi = 60^\circ$, they are almost equal at all load levels. On the other hand, for $\psi = 75$ and 90°, ψ_p^a for $\alpha = \beta = 20^\circ$ is more than the corresponding values computed for $\alpha = \beta = 0^\circ$. In fact, Fig. 7(c) shows that for $\psi = 90^\circ$, ψ_p^a attains a value between 105 and 115° which indicates that σ_{22} near the notch tip is compressive in nature. Interestingly, Chiang and Chai (1994) in their analysis of an adhesively bonded edge-notched flexure specimen under shear loading also observed that the mean stress in the layer ahead of the crack tip is negative.

It should be noted here that for $\psi = 90^\circ$, the remotely applied boundary conditions are antisymmetric with respect to the X_1-axis. But a value of ψ_p^a greater than 90° suggests that the near-tip solution is not antisymmetric. The reason for this counter-intuitive behaviour is explained below. As mentioned above, it was found that for an applied mode mixity of $\psi = 90^\circ$, a compressive stress state prevails in the region $X_2 \geq 0$, whereas, it is tensile in the lower part of the layer. Since for the pressure sensitive case, the material behaves differently in tension and compression (see Section 2.1), the antisymmetry of the

problem is lost. On the other hand, a von Mises material ($\alpha=\beta=0^\circ$), responds similarly in tension and compression and, consequently, the antisymmetric nature of the problem is preserved, as can be seen from Fig. 7(b).

The variations of ψ_p^a with normalised load for a pressure sensitive material with non-associated plastic flow ($\alpha=20^\circ$, $\beta=0^\circ$) are shown in Fig. 7(d) corresponding to different remote mixities ψ. On comparing Fig. 7(c) and (d), it can be observed that decrease in the flow parameter β reduces ψ_p^a at a given load for remote mixity ψ of 30 and 60°, but has little effect for $\psi=75^\circ$. The reduction in ψ_p^a for $\psi=30$ and 60° with decrease in β corroborates with the increase in the normal stress in the layer as mentioned in Section 3.3. It was observed that for remote mixity of $\psi=90^\circ$, the plastic mixity ψ_p varies strongly with

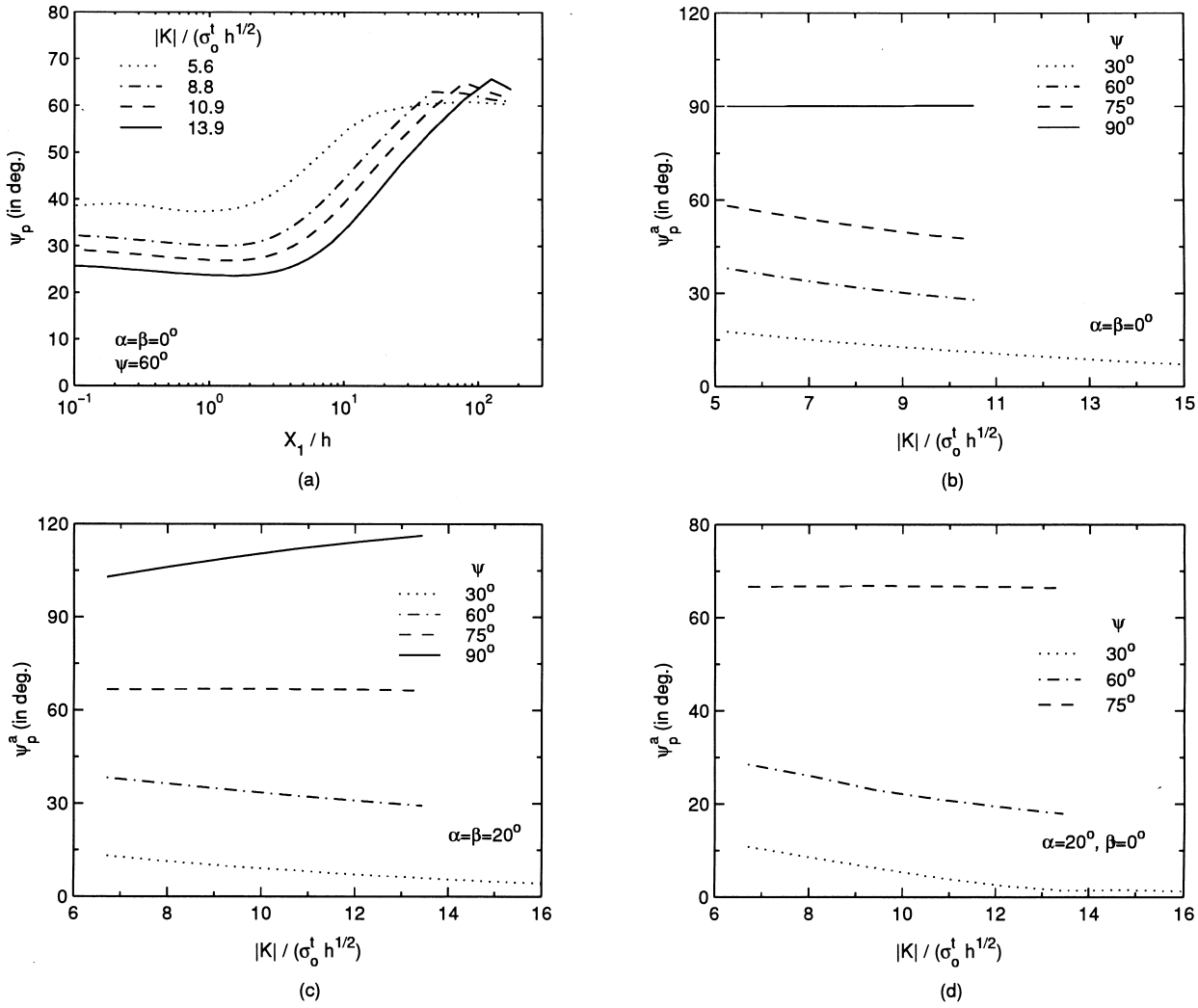

Fig. 7. (a) Variation of plastic mixity ψ_p with normalised distance X_1/h along the mid-plane of the adhesive layer for $\psi=60^\circ$ corresponding to different load levels. (b, c, d) Variations of asymptotic near-tip plastic mixity ψ_p^a with $|K|/(\sigma_0^t h^{1/2})$ for $\alpha=\beta=0^\circ$, $\alpha=\beta=20^\circ$ and $\alpha=20^\circ$, $\beta=0^\circ$, respectively.

distance ahead of the notch tip for the case $\alpha = 20^\circ$, $\beta = 0^\circ$, and does not attain a constant limiting value near the tip.

3.5. Notch tip deformation

In this section, the effect of pressure sensitivity of the adhesive layer and mode mixity on the notch tip deformation is investigated. To this end, following Ghosal and Narasimhan (1994), the linear distance between two points which were situated above and below the centre of curvature of the notch in the undeformed configuration (marked as P_0 and Q_0 in Fig. 1(c)), is defined as the notch tip deformation length and is denoted by d. The initial value of d is equal to b_0. It should be noted that under mixed mode loading, one portion of the notch blunts while the remaining part sharpens (see, for example, deformed notch shapes given by Ghosal and Narasimhan, 1994; Varias et al., 1992).

The variation of notch deformation $(d-b_0)$ normalised by (J/σ_0^t) with normalised load is shown in Fig. 8(a) and (b) for different values of α corresponding to the case of associated plastic flow. Here, $J = (1-\nu_s^2)|K|^2/E_s$ is the value of the remotely applied J integral. These figures pertain to remote mixity $\psi = 0$ and 60°, respectively. Fig. 8(a) shows that for $\psi = 0^\circ$, the normalised notch deformation $(d-b_0)/(J/\sigma_0^t)$ initially decreases with load and then reaches a steady value, whereas, for $\psi = 60^\circ$, the initial decrease is followed by a moderate increase before it attains a steady value (see Fig. 8(b)). The attainment of a constant value indicates that, on further increase of load, $(d-b_0)$ increases linearly with applied J. For the von Mises case, under Mode I, it can be seen from Fig. 8(a) that $(d-b_0) \approx 0.5(J/\sigma_0^t)$, which matches well with the results of Shih (1981) for an unconstrained homogeneous material. It can be observed from Figs. 8(a) and (b), that for both $\psi = 0$ and 60°, the parameter $(d-b_0)/(J/\sigma_0^t)$ increases with increase in α at a given load. This implies that pressure sensitivity enhances the deformation in the notch tip region. The above effect is stronger under Mode I loading (Fig. 8(a)).

In Fig. 8(c), the influence of the flow parameter β on normalised notch tip deformation for $\psi = 60^\circ$, corresponding to a fixed value of $\alpha = 20^\circ$, is shown. It can be observed from this figure that there is a significant enhancement in the notch tip deformation, at a given load, with a decrease in the value of β. The variation of $(d-b_0)/(J/\sigma_0^t)$ with normalised load for different levels of remote mode mixity ψ is shown in Fig. 8(d). This figure pertains to the case $\alpha = \beta = 20^\circ$. It can be noticed that for initial stages of loading, the normalised notch tip deformation is highest for $\psi = 0^\circ$ and decreases with increasing ψ. On the other hand, the steady state value reached by this normalised parameter (at large loads) shows the reverse trend and increases with the mode mixity parameter. The latter trend has been observed in earlier studies on homogeneous elastic–plastic solids under mixed mode loading (Ghosal and Narasimhan, 1994, 1997).

3.6. Fracture toughness due to interface debonding

For an adhesively bonded system, debonding at the interface is a very common failure mode (Riemanis et al., 1991; Chai, 1986). In their study on a pressure insensitive constrained layer, Varias et al. (1992) assumed that debonding occurs when the interface normal stress σ_{22} reaches a critical value. This assumption has the drawback that it ignores the role of the shear stress on the interface debonding process. In the present study, debonding is assumed to occur when the effective stress $\sigma_e = \sqrt{(\sigma_{22}^2 + f\sigma_{12}^2)}$, where f is a shear stress factor, reaches a critical value σ_f. Such a criterion has been employed by Camacho and Ortiz (1996) in order to simulate decohesion or brittle fracture in a variety of situations.

It is observed that the effective stress (σ_e/σ_0^t) undergoes a very similar variation along the layer as the normal stress (σ_{22}/σ_0^t). In particular, it attains a peak at several layer thicknesses away from the notch tip. This peak value is denoted here by σ_e^* and is a function of the load level. Varias et al. (1992) argue

from dimensional considerations that for a moderate load level, the parameter $|K|/(\sigma^* h^{1/2})$ varies linearly with $|K|/(\sigma_0^t h^{1/2})$, where σ^* is the maximum value attained in the layer by any stress measure σ. It is found in the present study that for $|K|/(\sigma_0^t h^{1/2}) \geq 3.5$, $|K|/(\sigma_e^* h^{1/2})$ does indeed vary linearly with $|K|/(\sigma_0^t h^{1/2})$. Further, following Varias et al. (1992), a relation of the nature,

$$\frac{|K|}{(\sigma_e^* h^{1/2})} = B + A\frac{|K|}{(\sigma_0^t h^{1/2})} \tag{11}$$

is assumed. The values of the constants A and B are obtained by curve fitting the above relation to the numerical results. In the following, the critical value $|K|_f/(\sigma_0^t h^{1/2})$ at fracture initiation is predicted using these values of A and B and assuming σ_f as σ_0^t and $2\sigma_0^t$.

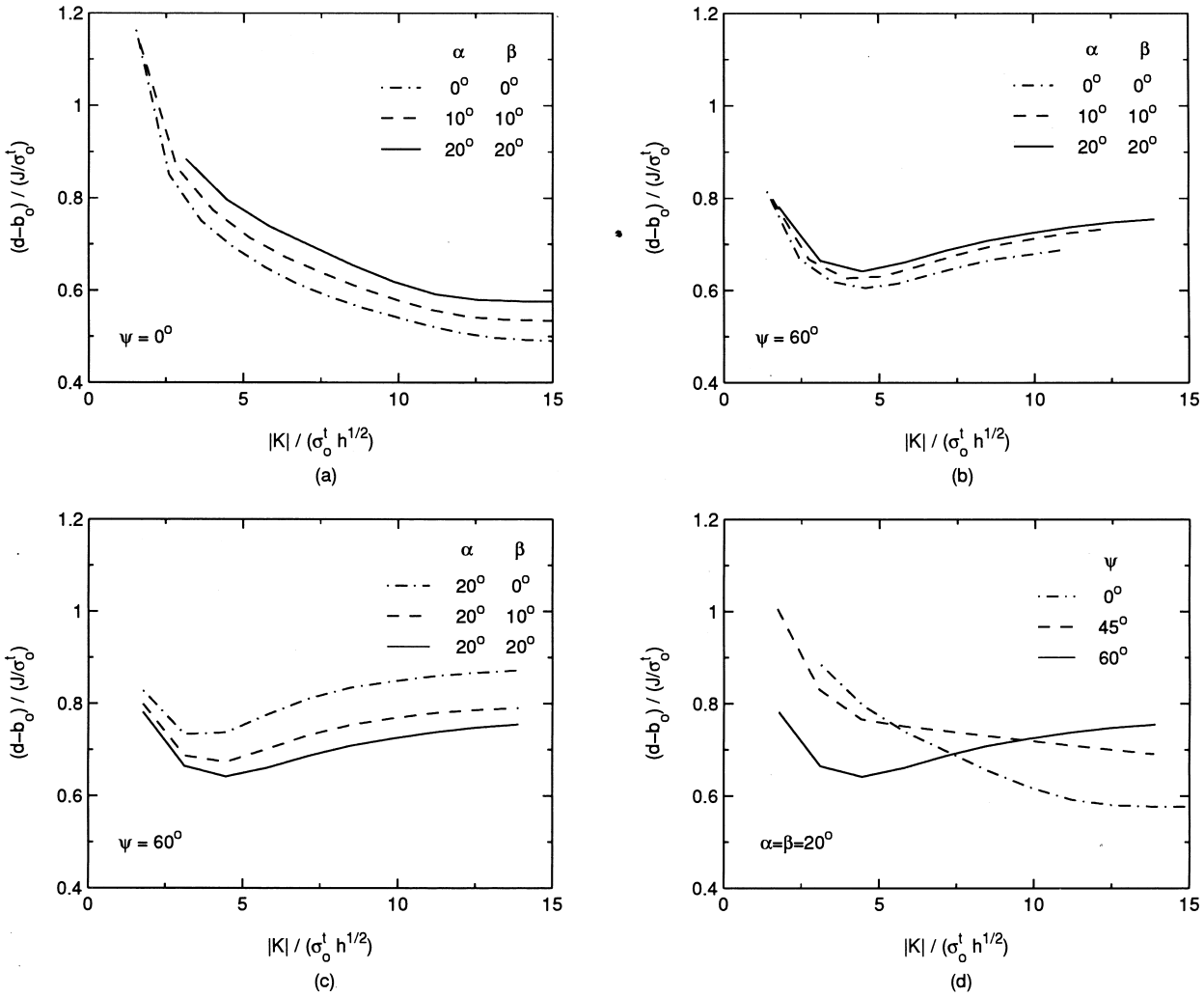

Fig. 8. Variations of normalised notch tip deformation $(d-b_0)/(J/\sigma_0^t)$ with normalised load $|K|/(\sigma_0^t h^{1/2})$ for different levels of α and β corresponding to (a) $\psi = 0^\circ$ and (b, c) $\psi = 60^\circ$. (d) Effect of mode mixity parameter ψ on $(d-b_0)/(J/\sigma_0^t)$ for the case $\alpha = \beta = 20^\circ$.

The variation of the fracture toughness for the interface debonding mechanism, as measured by the critical value of normalised load $|K|_f/(\sigma_0^t h^{1/2})$, with remote mode mixity ψ is shown in Fig. 9(a) and (b) for $f = 0$ and 2, respectively. Results are presented for $\alpha = \beta = 0^\circ$ and $\alpha = \beta = 20^\circ$ in these figures in order to assess the effect of pressure sensitivity of the adhesive layer on this variation. It can be observed from Fig. 9(a) and (b) that $|K|_f/(\sigma_0^t h^{1/2})$ increases with increase in mode mixity ψ. This is caused by the low levels of stresses prevailing in the interface region under mixed mode loading compared to Mode I (see Section 3.3). Similar variations in fracture toughness due to interface debonding with ψ was predicted for a metal–ceramic combination by Varias et al. (1992). Fig. 9(a) and (b) also show that, at a given mode mixity, $|K|_f/(\sigma_0^t h^{1/2})$ is higher for a pressure sensitive layer ($\alpha = \beta = 20^\circ$) than that for the pressure insensitive one ($\alpha = \beta = 0^\circ$), provided the same critical stress level can be used in both cases to indicate the onset of interface decohesion. This difference in the predicted fracture toughness increases with increase in the mode mixity parameter ψ. This is due to the fact that the percentage reduction in peak stress levels, when α is increased from 0 to 20°, is more pronounced for mixed mode loading than for the Mode I case (see Section 3.3). On comparing Fig. 9(a) and (b), it can be observed that for $\psi \geq 45^\circ$ (loading cases closer to Mode II), a lower toughness value is obtained for $f = 2$ compared to $f = 0$, due to higher levels of shear stress in the layer.

3.7. Effect of E/σ_0^c on stress and deformation fields

It was mentioned in Section 2.3 that the value of the material parameter E/σ_0^c chosen in this work is higher than that reported for polymers in the literature. Consequently, an investigation was undertaken to ascertain the effect of the above mentioned parameter on the results reported here. In Figs. 10(a) and (b), the normal stress variations with X_1/h are shown corresponding to two different load levels for materials with the same α and β, but with $E/\sigma_0^c = 300$ and 70. These figures pertain to $\psi = 0$ and 60°, respectively. It can be observed from these figures that E/σ_0^c has a negligible effect on both the magnitude and the distribution of stresses in the layer.

In Fig. 10(c), the variation of normalised notch tip deformation $(d-b_0)/(J/\sigma_0^t)$ is plotted with normalised load for two different values of E/σ_0^c for $\alpha = \beta = 15^\circ$. The variations exhibited by the

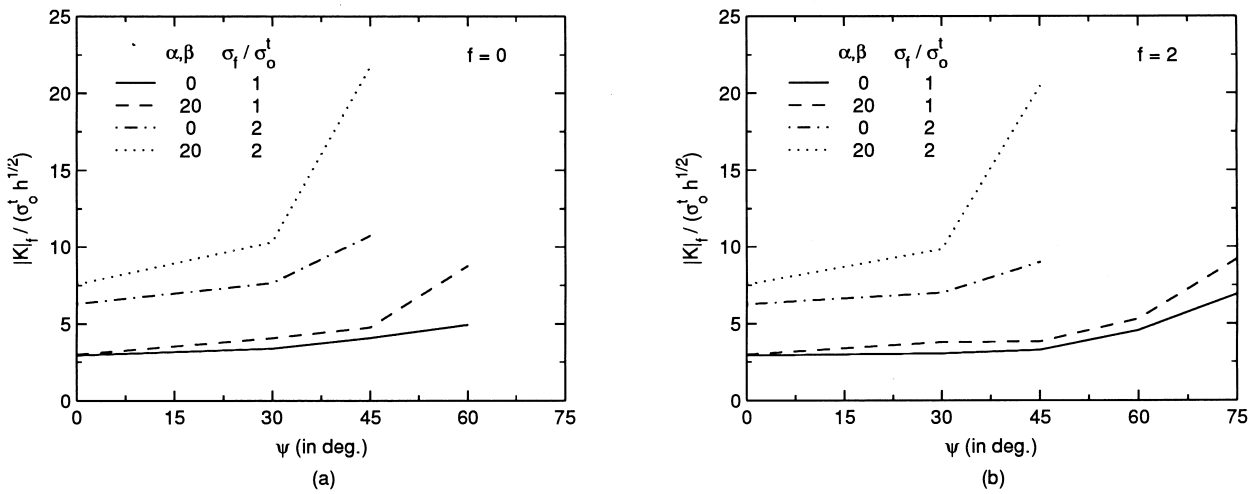

Fig. 9. Variations of normalised critical load due to interface debonding $|K|_f/(\sigma_0^t h^{1/2})$ with remote mode mixity parameter ψ for (a) $f = 0$ and (b) $f = 2$.

normalised notch tip deformation with load is very similar in the two cases, though their magnitudes are different. For example, the steady state value reached by the above parameter at high loads is about 25% higher for $E/\sigma_0^c = 70$ as compared to that for 300. This difference is roughly in agreement with that for a homogeneous material obeying the J_2 flow theory of plasticity and having a strain hardening index $n = 10$ (Shih, 1981). Thus, this investigation demonstrates that the parameter E/σ_0^c has very little effect on the stress distribution in the layer and, while the variation in notch tip deformation with load remains qualitatively similar, the magnitude changes in accordance with known behaviour (Shih, 1981).

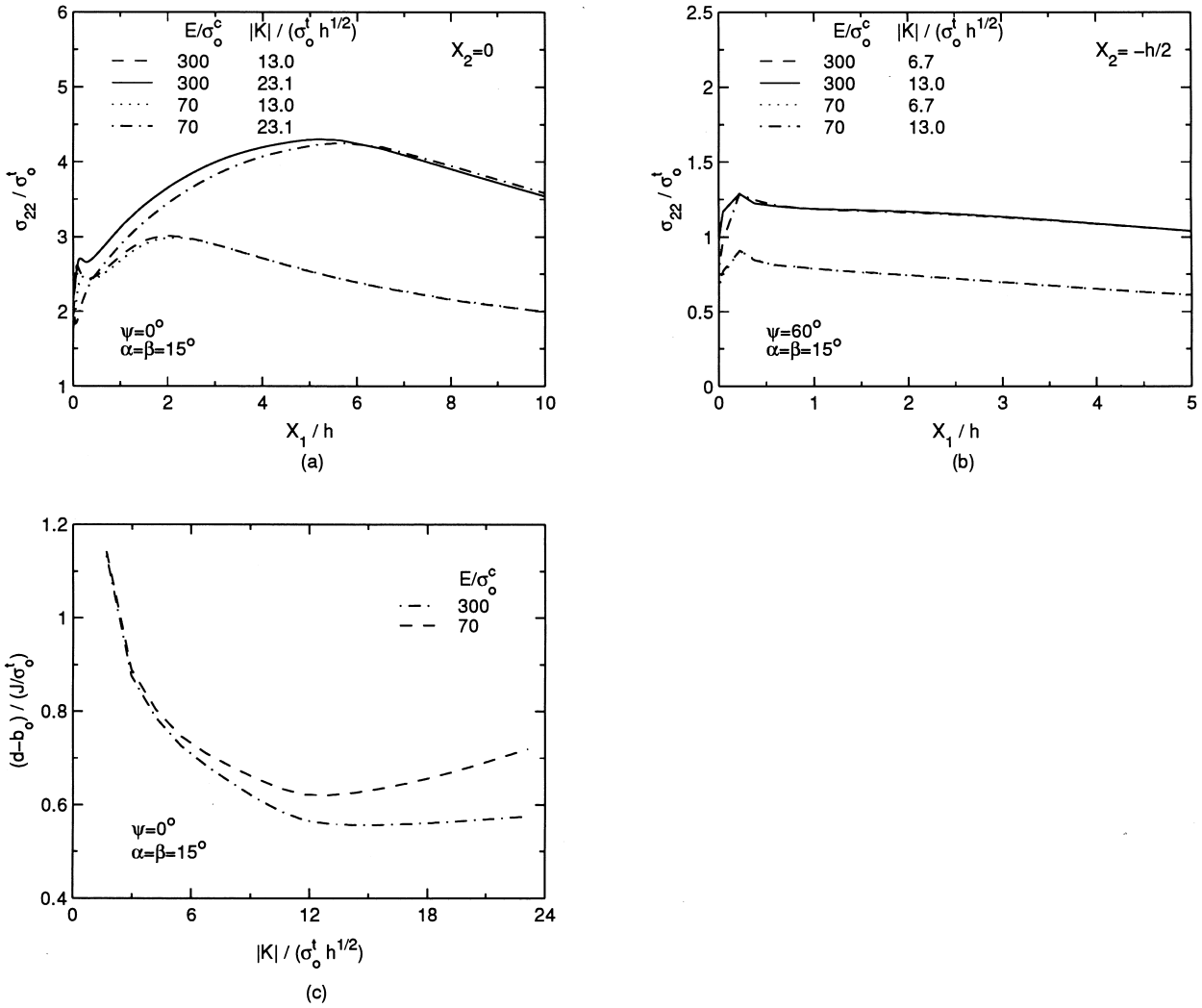

Fig. 10. Variations of normalised stress σ_{22}/σ_0^t with normalised distance X_1/h for $\alpha = \beta = 15^\circ$ and two values of E/σ_0^c corresponding to (a) $\psi = 0^\circ$ along the mid-plane of the adhesive layer and (b) $\psi = 60^\circ$ along the lower interface. (c) Variations of normalised notch tip deformation $(d-b_0)/(J/\sigma_0^t)$ with normalised load $|K|/(\sigma_0^t h^{1/2})$ for $\alpha = \beta = 15^\circ$ and mode mixity $\psi = 0^\circ$.

4. Conclusions

A numerical study of the stress and deformation fields near a stationary crack tip in an elastic–plastic adhesive layer attaching two elastically deforming adherends has been performed. A pressure sensitive yield criterion has been employed to idealise the behaviour of the adhesive. The main conclusions can be summarised as follows.

1. Under remote Mode I loading, the size of the plastic zone in the adhesive layer, at a given load $|K|/(\sigma_0^t h^{1/2})$, increases with an increase in the pressure sensitivity index α of the yield surface. The effect of pressure sensitivity on the plastic zone size is marginal for predominantly Mode II loading. Also, the plastic flow parameter β has little effect on the plastic zone size.
2. The existence of a second peak in the distribution of the stresses at distances several layer thicknesses away from the notch tip is a characteristic feature in a constrained ductile layer. This analysis shows that the nature of the peak, its location and magnitude are strongly influenced by the pressure sensitivity parameter α. In particular, with an increase in this parameter, the peak becomes more diffuse in nature, occurs at distances further away from the notch tip, and has a lower value. It is also found that, in general, all stress components in the adhesive layer drop with increasing pressure sensitivity of the yield surface. The plastic flow parameter β has little influence on the normal stress levels ahead of the notch tip for the Mode I case. On the other hand, under mixed mode loading, a decrease in β enhances the magnitude of the normal stress.
3. The mode mixity prevailing over a large distance ahead of the notch tip in the constrained ductile layer is different from both the remote elastic mixity and the corresponding near-tip plastic mixity in a homogeneous material. Moreover, the asymptotic plastic mixity level changes with the pressure sensitivity parameter of the yield surface, the plastic flow parameter, and the load level. Interestingly, a remotely applied antisymmetric load (Mode II), does not produce an antisymmetric near-tip field for a layer obeying the Drucker–Prager yield criterion.
4. The deformation of the notch tip increases with an increase in the pressure sensitivity of the yield surface. A non-dilational, non-associated flow causes even larger deformation.
5. Interface debonding is a common failure mode in adhesively joined bonds. It can be concluded from the present study that systems containing adhesive layers with larger pressure sensitivity would exhibit greater fracture toughness in such failures, provided similar critical stress levels govern the onset of interface decohesion.

Finally, it must be mentioned that the influence of pressure sensitivity on the results presented in Section 3 becomes more pronounced if the normalisations are performed using the compressive yield strength σ_0^c instead of σ_0^t. However, as explained in Section 3, it is more logical to employ σ_0^t for this purpose, since the layer experiences predominantly tensile loading for most of the analyses reported here.

Acknowledgements

The authors would like to gratefully acknowledge the Indian Space Research Organisation for financial support through the sponsored project ISTC/ME/RN/90. The first author also wishes to thank the Council of Scientific and Industrial Research, India for assistance provided through the fellowship 9/79(537)/95-EMR-I.

References

Abaqus/Standard User's Manual, 1996. Vol. 1, Version 5.6. Hibbit, Karlsson and Sorensen, RI, USA.

Akisanya, A.R., Fleck, N.A., 1992. Brittle fracture of adhesive joints. International Journal of Fracture 58, 93–114.

Argon, A.S., Andrews, R.D., Godrick, J.A., Whitney, W., 1968. Plastic deformation bands in glassy polystyrene. Journal of Applied Physics 39, 1899–1906.

Bauwens, J.C., 1970. Yield condition and propagation of Luders' lines in tension–torsion experiments on polyvinyl chloride. Journal of Polymer Science 8, 893–901 Part A-2.

Bowden, P.B., Jukes, J.A., 1972. The plastic flow of isotropic polymers. Journal of Materials Science 7, 52–63.

Brady, T.E., Yeh, G.S.Y., 1971. Yielding behavior of glassy amorphous polymers. Journal of Applied Physics 42, 4622–4630.

Brown, N., 1987. Engineered Materials Handbook, vol. 2. ASM International.

Camacho, G.T., Ortiz, M., 1996. Computational modelling of impact damage in brittle materials. International Journal of Solids and Structures 33, 2899–2938.

Chai, H., 1986. On the correlation between mode I failure of adhesives joints and laminated composites. Engineering Fracture Mechanics 24, 413–431.

Chai, H., 1992. Micromechanics of shear deformations in cracked bonded joints. International Journal of Fracture 58, 223–239.

Chai, H., 1993. Observation of deformation and damage at the tip of cracks in adhesive bonds loaded in shear and assessment of a criteria for fracture. International Journal of Fracture 60, 311–326.

Chiang, M.Y.M., Chai, H., 1994. Plastic deformation analysis of cracked adhesive bonds loaded in shear. International Journal of Solids and Structures 31, 2477–2490.

Chiang, M.Y.M., Chai, H., 1998. Finite element analysis of interfacial crack propagation based on local shear: Part I—Near tip deformation. International Journal of Solids and Structures 35, 799–813.

Dong, P., Pan, J., 1991. Elastic–plastic analysis of cracks in pressure sensitive materials. International Journal of Solids and Structures 28, 1113–1127.

Ghosal, A.K., Narasimhan, R., 1994. A finite element analysis of mixed-mode fracture initiation by ductile failure mechanisms. Journal of the Mechanics and Physics of Solids 42, 953–978.

Ghosal, A.K., Narasimhan, R., 1997. An approximate analysis of notch tip deformation under mixed-mode loading. Transactions of ASME, Journal of Applied Mechanics 64, 695–697.

Gurson, A.L., 1977. Continuum theory of ductile rupture by void nucleation and growth: Part I—Yield criteria and flow rules for porous ductile media. Journal of Engineering Materials and Technology 99, 2–15.

Hutchinson, J.W., 1968. Singular behavior at the end of a tensile crack in a hardening material. Journal of the Mechanics and Physics of Solids 16, 13–31.

Kanninen, M.F., Popelar, C.H., 1985. Advanced Fracture Mechanics. Oxford University Press, Oxford.

Li, F.Z., Pan, J., 1990a. Plane-strain crack-tip fields for pressure-sensitive dilatant materials. Transactions of ASME, Journal of Applied Mechanics 57, 40–49.

Li, F.Z., Pan, J., 1990b. Plane-stress crack-tip fields for pressure-sensitive dilatant materials. Engineering Fracture Mechanics 35, 1105–1116.

McMeeking, R.M., Rice, J.R., 1975. Finite element formulation for problems of large elastic–plastic deformation. International Journal of Solids and Structures 11, 601–616.

Pampillo, C.A., Davis, L.A., 1971. Volume change during deformation and pressure dependence of yield stress. Journal of Applied Physics 42, 4674–4679.

Quinson, R., Perez, J., Rink, M., Pavan, A., 1997. Yield criteria for amorphous glassy polymers. Journal of Materials Science 32, 1371–1379.

Rice, J.R., Rosengren, G.F., 1968. Plane strain deformation near a crack tip in a power law hardening material. Journal of the Mechanics and Physics of Solids 16, 1–12.

Riemanis, I.E., Dalgleish, B.J., Evans, A.G., 1991. The fracture resistance of a model metal/ceramic interface. Acta Mettalurgica et Materialia 39, 3133–3141.

Chowdhury, S.R., Narasimhan, R., 1995. Finite element simulations of ductile rupture in a constrained metal foil. Material Science and Engineering A191, 27–37.

Chowdhury, S.R., Narasimhan, R., 1998. Ductile failure in a constrained metal layer under mixed mode loading. Acta Materialia 46, 1103–1113.

Shih, C.F., 1974. Small scale yielding analysis of mixed mode plane-strain crack problems. ASTM STP 560, 187–210.

Shih, C.F., 1981. Relationship between the *J*-integral and the crack opening displacement for stationary and extending cracks. Journal of the Mechanics and Physics of Solids 29, 305–326.

Varias, A.G., Suo, Z., Shih, C.F., 1991. Ductile failure of a constrained metal foil. Journal of the Mechanics and Physics of Solids 39, 963–986.

Varias, A.G., Suo, Z., Shih, C.F., 1992. Mode mixity effect on the damage of a constrained ductile layer. Journal of the Mechanics and Physics of Solids 40, 485–509.

Wang, T.T., Zupko, H.M., Wyndon, L.A., Matsuoka, S., 1982. Dimensional and volumetric changes in cylindrical rods of polymers subjected to a twist moment. Polymer 23, 1407–1409.